Recent Progress in Dye-Sensitized Solar Cells for Improving Efficiency: TiO_2 Nanotube Arrays in Active Layer

Diptirani Behera [1], Tapas Bhanja [2], Madesi Rani Dora [3], PRAJNADIPTA SAHOO [4]
[1, 2, 3] Gandhi Institute for Education & Technology, Baniatangi, Khordha, Odisha
[4]NM Institute of Engineering & Technology,Bhubaneswar,Odisha
diptiranibehera@giet.edu.in, tapasbhanja@giet.edu.in, madesiranidora@giet.edu.in

Abstract: Dye-Sensitized Solar Cells (DSSC) were developed for several advantages, including: Low price/performance ratio, low manufacturing cost, wide-angle functionality and low incident light intensity, mechanical robustness and light weight are extensively studied. This paper summarizes recent advances in his DSSC technology to improve efficiency, focusing on the active layer of the photoanode, part of which is composed of dye and TiO film layers. In particular, this review article focuses on a number of studies reporting improved efficiency of his DSSCs using his TiO2 nanotubes, which show better electron transport. In conclusion, this paper suggests avenues for future research.

Keywords: Dye-Sensitized Solar Cells, photoanode, TiO.

1. Introduction

For nearly two centuries, mankind has employed fossil fuels as the primary energy source, and now we are facing serious problems as a result. Excessive emission of carbon dioxide and other greenhouse gases leads to environmental risk [1]. The price of fossil fuels continues to rise because of the increasing worldwide energy consumption. The need for an affordable, sustainable, and carbon-free renewable energy source is greater than ever, as the rapid growth rate of renewable energy consumption suggests [2,3].

Amongst all the renewable energy sources, solar energy has been regarded as very promising due to the abundance of its resource—sunlight—and the fact that it yields no harmful byproducts. The amount of solar energy that radiates upon earth in one hour is equivalent to the annual energy need of mankind [4]. Such high energy output, however, has not been achieved due to thermodynamic and technical constraints as well as few other reasons. Conventional commercial solar cells, which use crystalline and polycrystalline silicon, achieve over 20% energy conversion efficiency for residential end users [5]. However, there are some problems, such as complicated and difficult fabrication processing and high cost [6].

Dye-sensitized solar cells (DSSCs) are one potential alternative to silicon solar cells. DSSCs separate the light absorption and charge transfer processes, unlike Si-based cells. The organic dyes, or sensitizer molecules, adsorbed on the surface of the metal oxide nanostructure take the role of absorbing the incoming light, and the rest of the structure transfers the generated charge. An early version of a DSSC fabricated by O'Regan and Grätzel used ruthenium-based dye and 10-□m-thick porous TiO_2 nanoparticle films for the photoelectrode [7]. The cell yielded 7% power conversion efficiency (PCE), which was high enough to motivate further research on cells with similar structures. DSSCs provide several advantages, such as low price-to-performance ratio, low processing cost, ability to work at wide angles and low intensities of incident light, mechanical robustness, light weight, and aesthetically appealing transparent design. DSSCs have a number of remarkable properties that allow them to be used for several niche applications; they are low in

weight and able to display various colors and transparency, and they work effectively in a broad range of wavelengths [8, 9]. However, there are still several weaknesses that require improvement, such as relatively low efficiency, high cost of the ruthenium dyes, conducting glass, and platinum, temperature stability problems, and low scalability. Among the various potential solutions, some of the most widely investigated ones are the development of new sensitizers to cover a broader solar spectrum and the fabrication of new photoanode structures with enhanced light utilization. Studies have reported several different methods to improve the efficiency of DSSCs, such as the use of panchromatic sensitizers or 3-dimensional metal oxide nanostructures [10–14]. This review highlights another huge pool of studies that report improvements in the efficiency of DSSCs, especially those that employ the use of TiO_2 nanotubes. Moreover, we will introduce recent papers on high PCEs and the use of TiO_2 nanotube arrays in DSSCs. These papers describe the use of the space in TiO_2 nanotube array channels and how to overcome the barrier layer that exists at the bottom of these arrays to achieve a high PCE in DSSCs.

2. Principle of DSSCs

A DSSC consists of a photoelectrode, counter electrode, and electrolyte. The photoelectrode is made up of a transparent conductive oxide (TCO) glass substrate, a metal oxide such as mesoporous TiO_2 nanoparticles and a sensitizer such as ruthenium- (Ru-) complex dye. The electrolyte consists of a redox couple and diffusing reducing/oxidizing agent ions, and the counter electrode is coated with Pt as shown in Figure 1(a). In general, fluorine-doped tin oxide (FTO) glass is used on DSSCs instead of indium tin oxide (ITO) glass because of the better thermal stability at high temperatures [15]. During the sintering at 450–500° C, which crystallizes the mesoporous TiO_2 nanoparticles, the sheet resistance of ITO increases and affects the energy conversion efficiency of the DSSCs. However, the sheet resistance of FTO is independent of the temperature up to 500° C, which makes it favorable for applications that utilize the sintering step. TiO_2 nanoparticles are primarily used as electron acceptors on DSSCs that incorporate ruthenium dye. The counter electrode consists of FTO glass coated with platinum (Pt) or carbon to resist the oxidation and to work as a catalyst during the redox reaction in the electrolyte.

The principle of DSSCs is shown in Figure 1(b). When sensitizers absorb the light energy, and electrons are generated by the sensitizers and are transferred to the metal oxide films. During the hopping process in the metal oxide films, the generated electrons are transferred to the TCO and circulated. After the circulation, the sensitizers are reduced by an iodide redox process. In general, a Ru-complex dye is used as the sensitizer, and TiO_2 nanoparticles are used as the electron acceptors on DSSCs due to their high efficiency [20–22].

The energy diagram shown in Figure 1(c) demonstrates the electron transfer process of DSSCs. When the Ru-complex dyes absorb the light, the electrons change from the ground state to the excited state within a time on the order of nanoseconds (ns), as shown in the reaction (Figure 1(c)-(1)):

$$S^0 + h\rceil \; S^* \tag{1}$$

Although the detailed mechanism of the injection process is under debate, the electron injection from the Ru-complex dye into the conduction band of mesoporous TiO_2 nanoparticles takes about a femtosecond (fs) following the reaction shown in Figure 1(c)-(2). The energy level of electrons in the Ru-complex dye is higher than that of the conduction band of mesoporous TiO_2 nanoparticles, which enables the transfer of electrons into the mesoporous TiO_2 nanoparticles:

$$\begin{gathered} S^* \; S^+ + e^- \\ S^+ + e^- \; S^0 \end{gathered} \tag{2}$$

The excited state of the Ru-complex dye lasts around 20–60 ns, which is long enough for kinetic competition between electron injection and excited state decay in the Ru-complex dye.

The electrons injected into TiO_2 nanoparticles diffuse through mesoporous TiO_2 nanoparticles in about a millisecond (ms) in the reaction shown in Figure 1(c)-(3). However, when the injected electrons are trapped on mesoporous TiO_2 nanoparticles, they return to the oxidized Ru-complex dye by the reaction shown in Figure 1(c)-(4) or reduce the triiodide by the reaction shown in Figure 1(c)-(5). These processes are called as the recombination:

$$\begin{gathered} I_3^- + 2e^- \; I^- \text{ (Reduction)} \\ 3I^- \; I_3^- + 2e^- \text{ (Oxidation)} \end{gathered} \tag{3}$$

The Ru-complex dye is reduced by an iodide ion to accept the electron, as shown in the reaction in Figure 1(c)-(6):

$$2S^+ + 3I^- \; 2S^0 + I_3^- \tag{4}$$

The injected electrons on TiO_2 nanoparticles drive the external circuit and perform work, as in the reaction shown in Figure 1(c)-(7).

When the triiodide ion reduces to iodide to accept the electrons from the counter electrode by the reaction shown in Figure 1(c)-(8), the iodide ion causes the electron in the Ru-complex dye to return to the ground state, with the reaction shown in Figure 1(c)-(6).

Figure 1(d) illustrates the performance of DSSCs, and the solar power (□) can be calculated by the equation:

$$□ = □□. \tag{5}$$

The energy conversion efficiency of DSSCs is described by the ratio of the maximum electrical power output $□_{max}$ to the solar energy input □. The maximum electrical power output $□_{max}$ is calculated by the maximum current $□_{mp}$ and the maximum voltage $□_{mp}$:

$$□_{max} = □_{mp} \times □_{mp}. \tag{6}$$

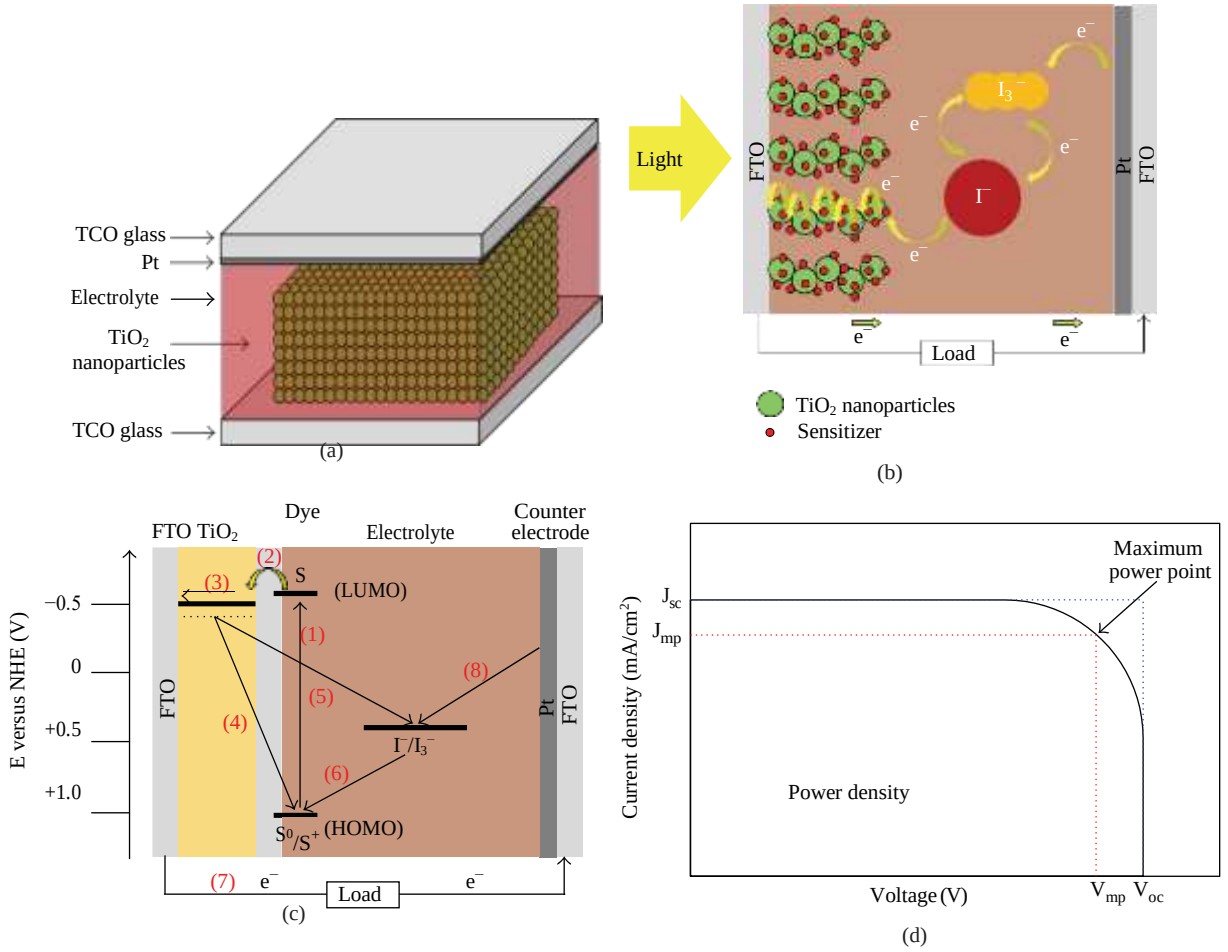

FIGURE 1: (a) Structure of DSSCs, (b) principle of DSSCs, (c) energy diagram of DSSCs, and (d) performance of DSSCs.

The solar power input is taken as the product of the irradiance of the incident light that is measured in W/m^2:

$$\square = \frac{\square_{max}}{\square}, \qquad \square = \frac{(\square_{mp} \times \square_{mp})}{\square}. \tag{7}$$

The fill factor □□ is a measure of the quality of the solar cell, and it can be calculated by comparing the maximum short- circuit current $\square_{sc}$ and maximum open-circuit voltage $\square_{oc}$ to the maximum current $\square_{mp}$ and maximum voltage $\square_{mp}$:

$$\square\square = \frac{(\square_{mp} \times \square_{mp})}{(\square_{sc} \times \square_{oc})}, \qquad \square = \frac{\square_{max}}{\square}, \qquad \square = \frac{(\square_{mp} \times \square_{mp})}{\square}, \qquad \square = \frac{(\square_{sc} \times \square_{oc} \times}{} \tag{8}$$

□ (100 mW/cm^2) is the solar cell testing standard under terrestrial conditions with air mass AM1.5.

The ideal power density of DSSCs is the product of $\square_{sc}$ and $\square_{oc}$. The maximum power density is the product of $\square_{mp}$ and $\square_{mp}$, and the difference between the two comes from the resistances of the cell, electrolyte, electrode, and other components. The energy conversion efficiency of DSSCs is related to the ideal power density and maximum power density as shown in Figure 2(a). When the fill factor is equal to 1, $\square_{sc}$ and $\square_{oc}$ are the same as $\square_{mp}$ and $\square_{mp}$. The series resis- tance $\square_{\square}$ includes the cell, electrolyte, electrode, and interface resistance. The increasing $\square_{\square}$ means that electrons are lost, so the voltage decreases earlier as shown in Figure 2(b).

The shunt resistance $\square_{sh}$ results from the recombination of electrons that are transferred in another way or are trapped by something. The decreasing $\square_{sh}$ means that there are few recombination sites, so the electrons are transferred to each layer as shown in Figure 2(c).

3. Dye

□□)

□

The dyes commonly used for DSSC applications share certain characteristics [23]: (i) excellent spectral absorption profile,

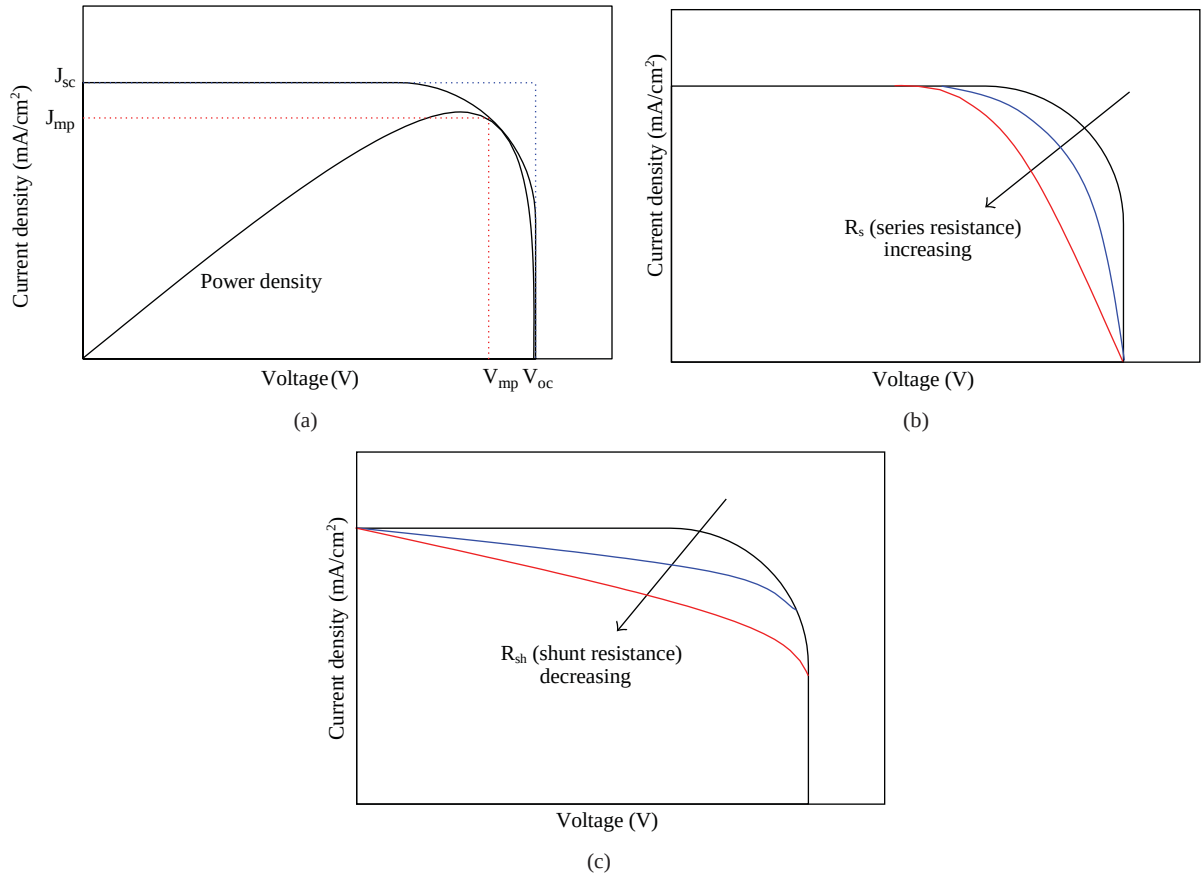

FIGURE 2: Characterization of DSSCs performance. (a) Ideal power density of DSSCs, (b) series resistance, and (c) shunt resistance.

like the panchromatic absorption; (ii) a surface-anchoring group, such as a carboxylate or phosphonate group; (iii) a LUMO matching the edge of the conduction band of the photoanode; (iv) a HOMO comparable to the electrolytes' Fermi level; and (v) the stability to endure 10^8 turnovers (20 years of exposure).

Generally, dyes fall into two categories: metal-complex-based polypyridyl dyes and metal-free organic dyes. While metal-complex—mostly ruthenium—dyes show high efficiencies due to high absorbance ranges extending to the near-infrared range, the metal-free organic dyes appeal to the market with their low processing cost and limited Ru requirements.

Metal-Complex-Based Dyes. Metal-complex dye sensitiz- ers generally consist of a central metal ion and a subsidiary ligand, typically a bipyridine or tetrapyridine that contains anchoring groups. The central metal ion performs the light absorbance. Subsidiary ligands can be structurally modified to fine-tune the photovoltaic properties.

Ruthenium complexes, as shown in Figure 3, have demonstrated excellent photovoltaic properties, such as broad absorbance profiles and well-fitted energy levels [24]. These factors, combined with electrochemical stability, make Ru complexes unrivaled for sensitizer uses [10, 25, 26]. One representative Ru-based dye is the N3 dye, whose reported conversion efficiency is over 10%.

Another one is N749 dye, which is called the black dye due to its enhanced absorption spectrum. It shows an enhanced efficiency as high as 10.4%. Recent research on this family of dyes includes the work conducted by Robson et al., in which the NCS ligands of the black dye were replaced with anionic tridentate chelating ligands to adjust the HOMO and LUMO of the dye sensitizers to increase the photocurrent without compromising other DSSC properties [27]. When a triphenylamine group was substituted for the NCS group and a phenyl-bipyridine-OMe group was used as the chelating ligand, an 8.02% PCE was measured.

There have been attempts to use metals other than Ru as the dye sensitizer. Such metals include Os [28], Re [29], Fe [30–32], Pt [33–36], and Cu [37, 38]. Os(II) complexes have better absorption spectra compared to Ru complexes. However, Alebbi et al. reported a lower energy conversion efficiency, attributing it to the slower electron transfer from the iodine electrolyte to the osmium complex [39]. Pt(II) diimine-dithiolate complexes showed a high IPCE of 47% at 500 nm [33] but had a poor light absorption capacity at longer wavelengths. The tenability of photophysical properties, due to possible structural modification of the substituents on the diimine and dithiolate, was notable. Cu(I) complexes have very similar photophysical properties to Ru complexes.

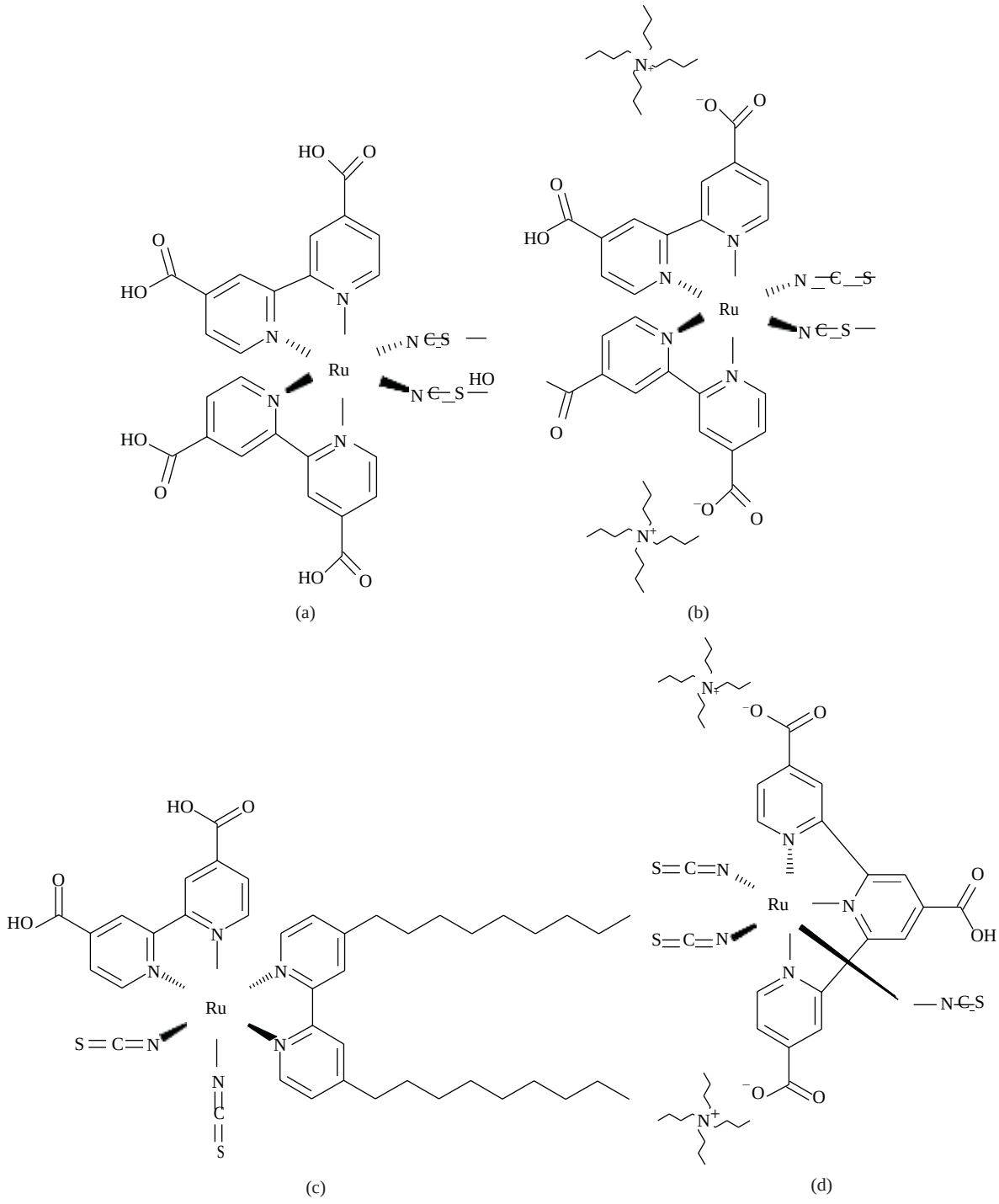

FIGURE 3: Ru-based dyes. (a) N3, (b) N719, (c) Z907, and (d) N749.

According to Constable et al., the □-□ characteristic of these complexes was sensitive to the location of the conjugated pi- bond.

Polyphyrins are also of interest due to their good absorption and stability. With zinc-polyphyrin dye and a Co(III) tris(bipyridyl)-based redox electrolyte, Yella et al. reported a breakthrough efficiency of 12.3% and attributed this high efficiency to the suppression of electron backtransfer by the dye structure [40].

Metal-Free Organic Dyes. N3 and N719 dyes exhibit high performances with very fast electron injections. However, the molar extinction coefficients in the visible and near-IR ranges

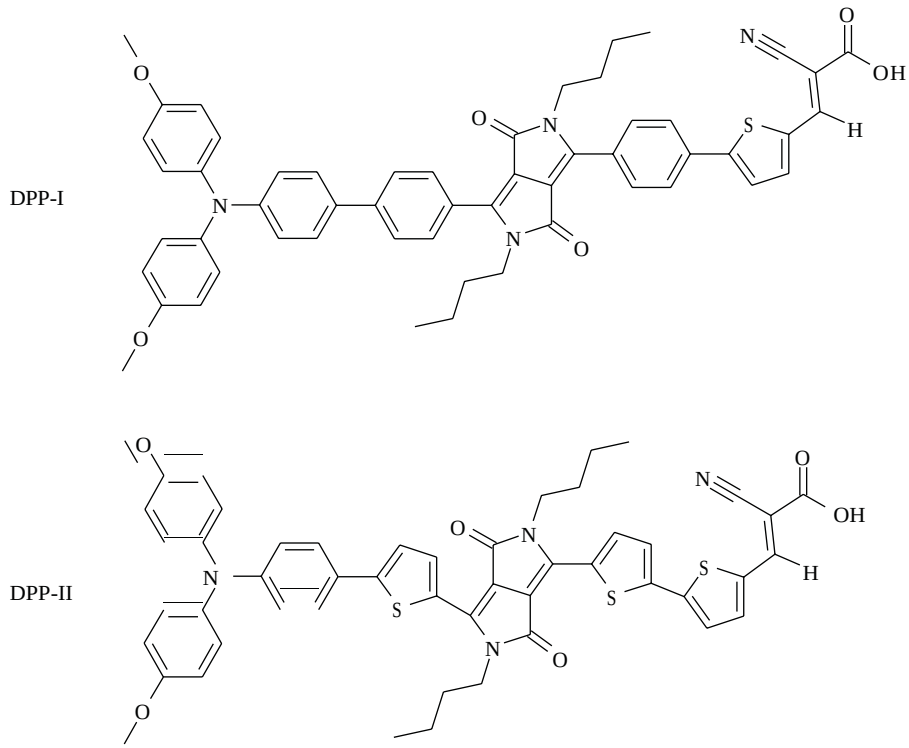

FIGURE 4: DPP-based dyes' molecular structures. Reprinted from [42].

are relatively low. Moreover, there are concerns about the cost effectiveness of ruthenium and the environmental impacts.

Organic dyes also enable easy synthesis and design of the dye molecules. The predominant structure of metal-free organic dyes is the donor-□-acceptor (D-□-A) structure. It works as a basic template to design new dye molecules by adjusting the functional group or the whole moiety of the donor, pi-bridge, or acceptor of an existing dye.

Zhang et al. reported a high power conversion efficiency of 11.5–12.8% with cyclopentadithiophene-benzothiadiazole derivatives [41]. This research group cografted the dyes having poor light absorption abilities, by which they successfully removed the penetration channels for Co(III) redox ions and thereby restricted the charge recombination at the titania surface. The dyes they used contain triphenylamine and benzoic acid moieties on each end of the cyclopentadithiophene-benzothiadiazole group, where different orders of the moieties generate two different dyes. The high PCE of 12.8% is even comparable to the Ru-based dyes, which proves that metal-free organic DSSCs can be as efficient as conventional DSSCs and sets a new standard for organic DSSCs for peer researchers.

Another approach taken by Qu et al. studied the diketopyrrolopyrrole (DPP) dyes and their photovoltaic characteristics as shown in Figure 4 [42]. These dyes commonly had a triphenylamine donor, carboxylic acid acceptor, and DPP pi-bridge. The introduction of DPP moieties improved the spectral absorption at longer wavelengths. The PCE was 3.44%, relatively high, and was attributed by the authors to high dye aggregation and electron recombination. Adding 1.5 mM of chenodeoxycholic acid (CDCA) partly resolved the aggregation issue and raised the PCE to 4.14%, with $\square_{sc}$ = 9.78 mA cm^{-2}, $\square_{oc}$ = 0.605 V, and a fill factor of 0.7 under AM1.5 solar light and with an iodine electrolyte.

Another approach to DSSC dyes involves extracting the natural dyes and structurally adjusting them for solar cell applications [49]. None of them so far has led to a PCE significantly higher than those of other organic dye sensitizers. One reason for their low PCEs is thought to be the low interaction between the dyes and TiO_2. High adsorption of dyes onto the TiO_2 structure is vital for high $\square_{oc}$, because electron recombination can occur. In fact, most of the natural dye-based DSSCs suffer from low $\square_{oc}$. Low stability of natural dyes is another issue. Therefore, improvements either in $\square_{oc}$ or in stability are essential in order to justify further studies
using this approach.

4. Metal Oxide

Metal oxide nanostructures have also been integrated into DSSCs to maximize the number of adsorbed dyes and thereby maximize the photocurrent. O'Regan and Grätzel used a mesoporous layer of TiO_2 to produce a 1000-fold increase in the surface area [7]. TiO_2 NPs are generally preferred for DSSC applications due to their high stability. The group also studied various alternatives, such as ZnO, SnO_2, or Nb_2O_5 [50], which were chosen because their energy band structures

are similar to that of TiO_2. However, these alternatives rarely yielded PCEs comparable to those of TiO_2-based cells [51].

TiO_2 Nanoparticle Films Based DSSCs. TiO_2 has three types of crystallinities: anatase, rutile, and brookite. A com- parative study between anatase and rutile TiO_2 nanoparticle films was conducted by Park et al. [52]. This study concluded that the anatase TiO_2 nanoparticles have better electron transport than do rutile TiO_2 nanoparticles in DSSCs.

While nanoparticle films have shown significantly higher PCEs compared to those of other nanostructures, due to their excessive number of adsorbed dyes, they have a clear disadvantage in charge transport. In nanoparticle films, the generated charge has to pass several nanoparticles before it reaches the substrate. Since the particles slightly differ in their energy states, the combined energy band might contain several trap states, and the charge may be trapped in such states, losing the energy and delaying the charge transfer process [53]. Moreover, the grain boundary between nanoparticles is not effective for electron transport.

In TiO_2 nanotubes, the electron transport is better than TiO_2 nanoparticles due to the absence of a grain boundary. However, the small surface area for sensitizers is one of the main obstacles to achieving a high PCE in DSSCs. Toretain the advantage in the surface area while improving the charge transport, numerous studies have been conducted to test DSSCs based on TiO_2 nanotubes.

TiO_2 Nanotube Arrays

Titanium Anodization. Anodic titanium oxide TiO_2 nanotube arrays have properties that make them more effective than many other forms of TiO_2 for applications in photocatalysis [54, 55], gas sensors [44, 56–59], photoelectrolysis [60–62], and photovoltaics [63–65]. Since Zwilling reported on the TiO_2 nanotube arrays in chromic acid and hydrofluoric acid in 1999 [66], TiO_2 nanotube arrays have been studied in terms of fabrication, characterization, application, and formation mechanism [44, 67].

Gong et al. reported on TiO_2 nanotube arrays in a 0.5 wt% HF aqueous solution at room temperature using different anodizing voltages [68]. The film thickness could not be increased above 400–500 nm when an HF-based electrolyte was used. The fluoride solution dissolves TiO_2 by forming TiF_6^{2-} anions. The acidity of HF electrolytes is too high and results in a rapid dissolution of TiO_2. To overcome this problem, Mor et al. reported that the addition of acetic acid to a 0.5 wt% HF electrolyte in a 1 : 7 ratio resulted in more mechanically robust TiO_2 nanotube arrays without changing their shape or size [57, 69]. The surface morphology of TiO_2 nanotube arrays anodized in an electrolyte containing 2.5% HNO_3 and 1% HF at 20 V for 4 hours exhibited a uniform, clean, and regular TiO_2 nanotube array structure with a length of about 400 nm as reported by Ruan. The anodization with an electrolyte composed of 0.5 M H_3BO_3, 2.5% HNO_3, and 1% HF at 20 V for 4 h led to irregular pore of TiO_2 nanotube arrays but a long length of about 560 nm [70]. To increase the length of the TiO_2 nanotube arrays, Ti was anodized with KF or NaF in the electrolyte [71]. The acidity of the electrolyte could be controlled by adding HF, H_2SO_4, or Na_2SO_4 to adjust the balance of the dissociation of TiO_2 at the electrolyte/oxide interface and the oxidation of TiO_2 at the oxide/metal interface [72, 73].

Grimes et al. obtained TiO_2 nanotube arrays up to approximately 1000 □m using a variety of organic electrolytes, such as dimethyl sulfoxide, formamide, ethylene glycol, and N-methylformamide [74–76].

The key to constructing longer TiO_2 nanotube arrays is to reduce the water content in the anodization bath to less than 5%. In organic electrolytes, a little water content reduces the dissociation of the oxide in the fluorine-containing electrolytes.

The chemical reaction of titanium anodization should be the same as that of aluminum anodization [44, 74, 77, 78]. The key processes are the growth of an anodic TiO_2 when the surface of Ti is oxidized with oxide anion and the dissociation of oxide anions through dissociation and field-assisted dissolution in water, as shown in Figure 5 [43]. At the electrolyte/oxide interface, the reaction is written as

$$H_2O \rightarrow OH^- + H^+ \quad \text{or} \quad OH^- \rightarrow O^{2-} + H^+ \tag{9}$$

The cations move to the cathode and undergo the reaction:

$$2H^+ + 2e^- \rightarrow H_2 \tag{10}$$

The oxide ions, OH^- or O^{2-}, migrate through the oxide layer to form TiO_2:

$$Ti + □OH^- \rightarrow Ti(OH)_□ + □e^- \quad \text{or} \quad Ti + 2O^{2-} \rightarrow TiO_2 + 4e^- \tag{11}$$

where □ is yet to be determined. Titanium hydroxide decomposes to form TiO_2 at the oxide/hydroxide interface. F^- in the electrolyte moves to the anode and undergoes the reaction:

$$TiO_2 + 6F^- + 4H^+ \rightarrow [TiF_6]^{2-} + 2H_2O \tag{12}$$

The overall reaction of TiO_2 nanotube arrays is

$$TiO_2 + □H_2O + 6F^- \rightarrow TiF_6]^{2-} + (□+2-□)O^{2-} + □OH^- + (2□-□)H^+ \tag{13}$$

where □ was introduced to indicate the ratio of the dissocia- tion rate of water to the dissolution rate of TiO_2.

Pores develop from pits on the Ti plate surface, and a schematic diagram for the equifield strength model is shown in Figure 6.

The initiation and growth of pores are associated with accelerated dissolution of TiO_2 due to the influence of an electric field [79]. Many defects, such as impurities, dislocation, grain boundaries, or nonmetallic inclusions, could cause a faster dissolution rate and lead to pit growth [80, 81]. When Ti^{4+} cations escape from the oxide surface because of an applied field, Ti^{4+}cation vacancies can appear and accumulate to form high-density voids in the oxide layer, which can aid in the propagation of pits [82,83].

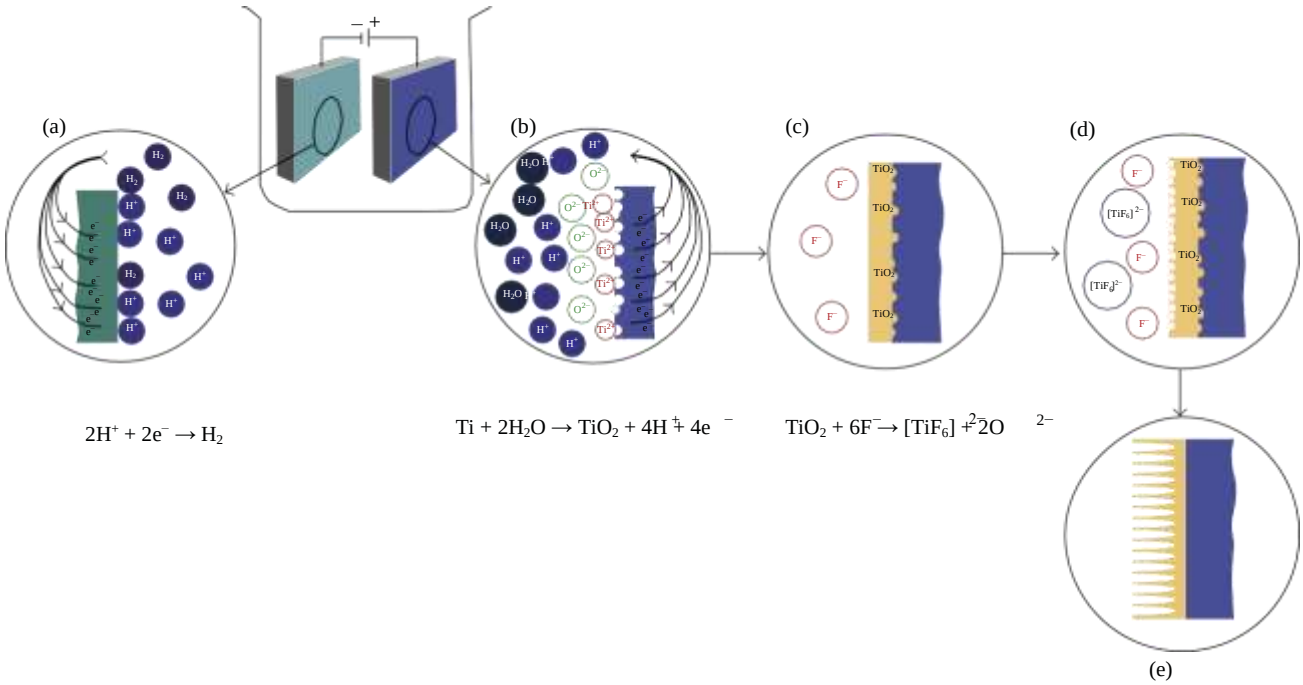

FIGURE 5: Growth of regular TiO_2 nanotube arrays: (a) cathodic reaction, (b) anodic reaction, (c) transition state of TiO_2 layer, (d) beginning of nanotube formation, and (e) TiO_2 nanotube arrays. Reprinted with permission from [43]. Copyright 2012, Elsevier.

TiO_2 Nanotube Arrays Based DSSCs. Grimes et al. reported backside-illuminated DSSCs based on TiO_2 nan- otube array electrodes in 2006. They were based on 6 □m long, highly ordered nanotube-array films sensitized by a self- assembled monolayer of N719 sensitizer which showed an 8.79 mA cm^{-2} short-circuit current density, an 841 mV open-circuit potential, and a 0.57 fill factor, yielding a PCE of 4.24% under AM1.5 sun. This investigation was the first attempt to construct a DSSC of TiO_2 nanotube arrays. However, it used backside illumination. Therefore, incident sunlight had to pass a Pt-coated counter electrode and electrolyte that absorbed light near 400 nm. To increase the energy conversion efficiency using TiO_2 nanotube arrays in DSSCs, the structure should be designed with front illumination.

Several approaches using TiO_2 nanotube arrays in DSSC designs have incorporated a thin film consisting of TiO_2 nan-otube arrays with the photoanode of the DSSCs, improving the scattering-driven light harvesting and suppressing the charge recombination. Park et al. reported a simple method for preparing TiO_2 nanotube arrays on the FTO glass [16]. In this method, a thin film of TiO_2 was anodized with NH_4F to form an array of TiO_2 nanotubes. The nanotube array was then detached from the metallic Ti substrate by the use of an HCl solution and was annealed onto a sheet of FTO glass at 500° C for 30 min. The photoanode fabricated with this method was equipped with a Pt counter electrode, $Ru(II)LL(NCS)_2$ dye (L = 2,2-bipyridyl-4,4-dicarboxylic acid; L = 2,2-bipyridyl-4,4-ditetrabutylammonium carboxy-late), and an iodine electrolyte to yield 7.6% power conversion efficiency under 1 sun illumination.

Chen and Xu produceda crystalline TiO_2 nanotube array thin film [17]. The crystalline TiO_2 nanotube arrays were usually obtained by annealing the array at a high temperature, and the high-temperature annealing caused the TiO_2 nan-otube arrays to curl. The researchers circumvented this prob-lem by introducing an additional step of anodization after annealing, which results in a double-layer structure of TiO_2 nanotube arrays, in which the lower layer is later dissolved in an H_2O_2 solution. The resulting free-standing TiO_2 nanotube arrays did not need any support to maintain their crystal structure, enabling them to be attached to FTO glass and to fabricate a front-illuminated DSSC. The front illumination of the DSSC enhanced the irradiation intensity by 11% compared to the conventional back-illuminated method. Additionally, the crystalline free-standing TiO_2 nanotube arrays provided a longer electron lifetime, which caused the PCE to increase from 2.8% with a back-illuminated DSSC equipped with thick TiO_2 nanotube arrays on a Ti substrate to 5.5% with a front-illuminated, crystal-structured, TiO_2 nanotube array-based DSSC.

Lin et al. fabricated open-ended TiO_2 nanotube arrays, which differed from the previously mentioned nanotube structures in that there was no blocking layer of TiO_2 at the junction point between the FTO glass and the TiO_2 nanotube arrays [18]. The DSSC devices were fabricated with the open-ended TiO_2 nanotube arrays interconnected to the FTO glass by NP-TiO_2 paste, N719 dyes, Pt-FTO glass, and an iodine-based electrolyte for front-side illumination. The open-ended nanotube arrays were prepared by the simple introduction of an oxalic acid solution as an etching agent. Compared to the close-ended TiO_2 nanotube arrays, the open-ended TiO_2 nanotube arrays dramatically increased the short-circuit current, resulting in a high PCE of 9.1%. The increase in the short-circuit current was attributed by the authors to

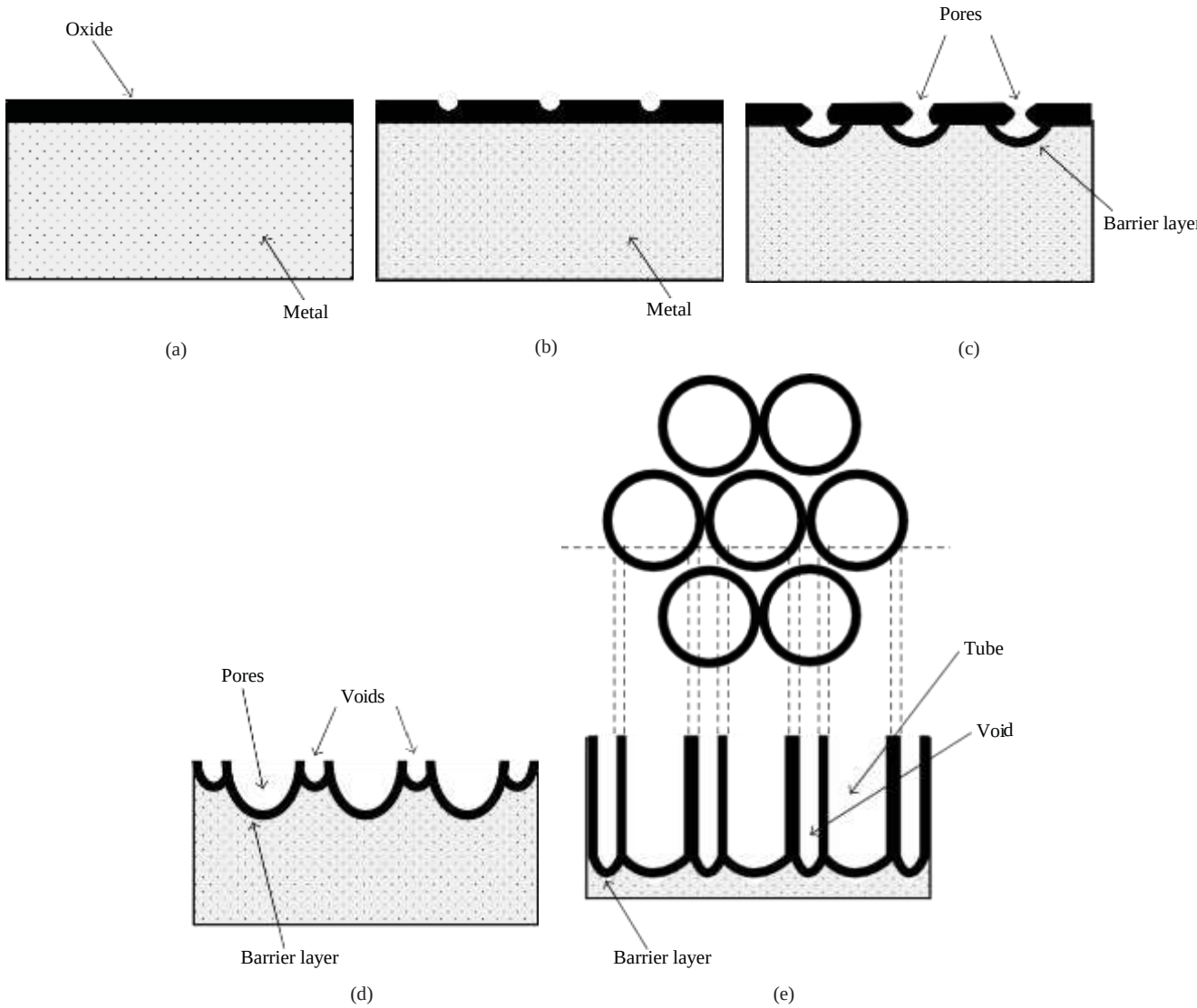

FIGURE 6: Schematic diagram of the evolution of a nanotube array at constant anodization voltage: (a) oxide layer formation, (b) pit formation on the oxide layer, (c) growth of the pits into scallop-shaped pores, (d) metallic part between the pores undergoing oxidation and field-assisted dissolution, and (e) fully developed nanotube array with a corresponding top view. Reprinted with permission from [44]. Copyright 2006, Elsevier.

the enhanced interaction between the electrolyte and NP-TiO_2 underlayer due to the absence of the bottom caps. The open-ended nanotube array showed a strong enhancement in capturing incident photons with longer wavelengths, which also indicated that opening the tube bottom enabled the DSSC device to collect the excited electrons over the entire length of the nanotubes.

Li et al. reported on the fabrication of crystalline TiO_2 nanotube arrays using the secondary anodization step in a similar manner to Chen et al. [17, 19]. With these free-standing crystalline TiO_2 nanotube arrays, they used a dry-etching method with a plasma reactor under BCl_3/Cl_2 to make the nanotube bottom open-ended and compared this array to a close-ended nanotube array fabricated with the same methodology, but without the etching step. The resulting PCE was higher for the open-ended nanotube arrays (6.24%) than it was for the close-ended nanotube arrays (4.84%). The authors explained this difference as the result of the interface between nanotube arrays and FTO being more compactly adhered, leading to improved electron diffusion and charge collection. This conclusion is similar to that of Lin et al.

The open-ended TiO_2 nanotube arrays generally show a better photoelectric performance than do the close-ended nanotube arrays. Rho et al. studied the effect of the thickness of the bottom cap (barrier layer) of the nanotube arrays, as shown in Figure 7 [45]. The authors fabricated the TiO_2 nanotube arrays with two anodization steps, followed by ion milling with argon ions. The thickness of the barrier layer was controlled by varying the time for the ion-milling step. The resulting PCEs varied from 2.5% to 3.7%. As the barrier layer was removed, the PCE increased. When the DSSC

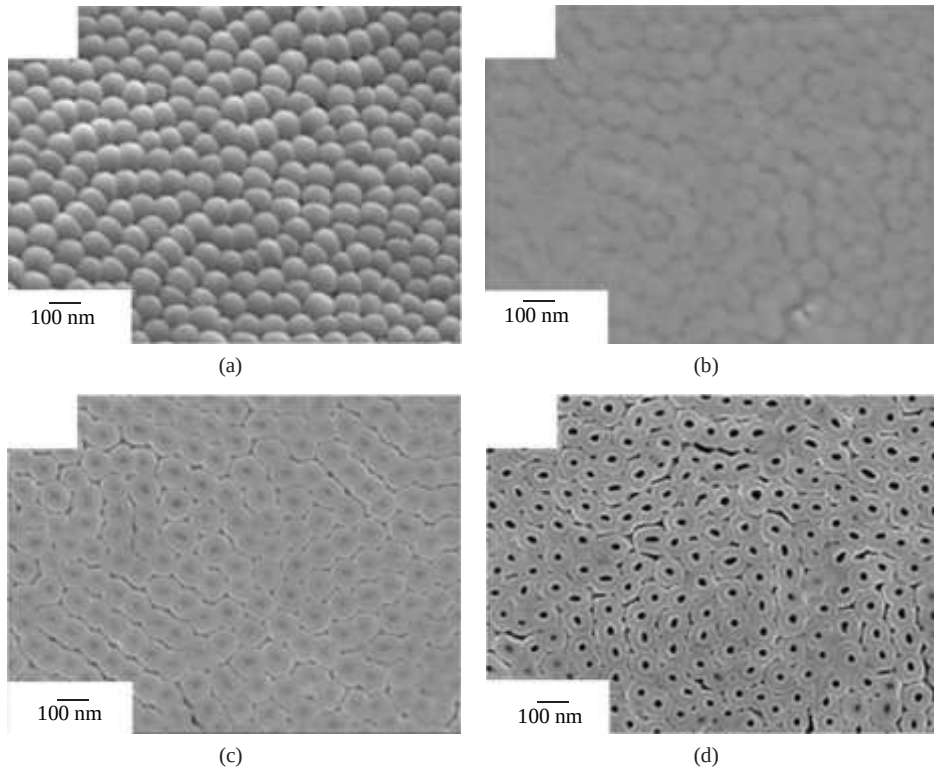

FIGURE 7: SEM images taken by Rho et al. of the freestanding TiO_2 films after ion milling of (a) 0, (b) 20, (c) 30, and (d) 90 minutes. Reprinted with permission from [45]. Copyright 2012, American Chemical Society.

was designed with back-side illumination, the efficiency was lower than when it was designed with front-side illumination. In back-side illumination, the existence of the barrier layer does not affect the incident light intensity, as the light reaches the barrier layer after it is absorbed by the dye molecules. Rather, in this case, the more decisive factor influencing the conversion efficiency was the efficiency of electron diffusion, as the barrier layer may significantly hinder the electron transport.

The energy conversion efficiency of DSSCs based on open-end TiO_2 nanotube arrays was much higher than the efficiency based on closed-end ones. This result means that the barrier layer, corresponding to the under layer of the detached TiO_2 nanotube arrays, has a marked effect on the conversion efficiency, since the barrier layer has been removed in open-end TiO_2 nanotube arrays but left intact in closed-end TiO_2 nanotube arrays. The barrier layer could affect the conversion efficiency by preventing the diffusion of materials like electrolytes and dye molecules, by reducing the transmittance of light, and by hindering the electron transport. The electrons generated by excitation of the dyes adsorbed on the TiO_2 nanotube arrays could transfer to the electrode through the TiO_2 nanotube arrays. In this case, they must pass the barrier layer to reach the electrode. (DSSCs with free-standing TiO_2 nanotube array were summarized in Table 1.)

Development of TiO_2 Nanotube Arrays for DSSC. The various approaches mentioned in the earlier sections exploited TiO_2 nanotube arrays to achieve DSSC systems with higher efficiencies. Generally, the techniques to increase the efficiencies of TiO_2 nanoparticle systems can be also applied to TiO_2 nanotube systems. For example, combining plasmonic enhancement and/or $TiCl_4$ could benefit TiO_2 nanotube arrays, which have large spaces in them.

(1) Plasmonic TiO_2 Nanotube Arrays for DSSCs. Plasmonic solar cells are photovoltaic devices that use noble metal surface plasmons. Most solar cells have weak absorbers. To absorb larger amounts and longer wavelengths of incident light, the morphology of the substrate is etched with pyramids with sizes of 2–10 □m to obtain a wavelength-scale texture. This structure improves the light trapping for solar cells but increases the surface recombination and reduces the material quality [84, 85].

There is another approach involving the use of noble metal nanoparticles in solar cells. The light can be absorbed and scattered from the noble metal nanoparticles that are excited at the surface plasmon resonance.

The mechanism of plasmonic solar cells can be used to explain the photocurrent enhancement by metal nanoparticles incorporated into or on solar cells, as shown in Figure 8 [46]. One is scattering from the metal nanoparticles, which can be used as subwavelength scattering elements to couple and trap plane waves propagating from the Sun into the semiconductor thin film, by folding the light into a thin absorber layer as shown in Figure 8(a).

Light is preferentially scattered and trapped in the semiconductor thin film by multiple high-angle scatterings,

TABLE 1: Summary of DSSCs with free-standing TiO_2 nanotube arrays.

Year	Types of free-standing TiO_2 nanotube arrays after being detached from Ti plate	$\square_{oc}$ (V)	$\square_{sc}$ (mA/cm^2)	□□	PCE (%)	Reference
2008	Closed-ended and without crystallinity	0.733	16.8	0.62	7.6	[16]
2009	Closed-ended and with crystallinity	0.701	12.4	0.63	5.5	[17]
2010	Open-ended and without crystallinity	0.770	18.5	0.64	9.1	[18]
2011	Open-ended and with crystallinity	0.75	12.78	0.65	6.24	[19]

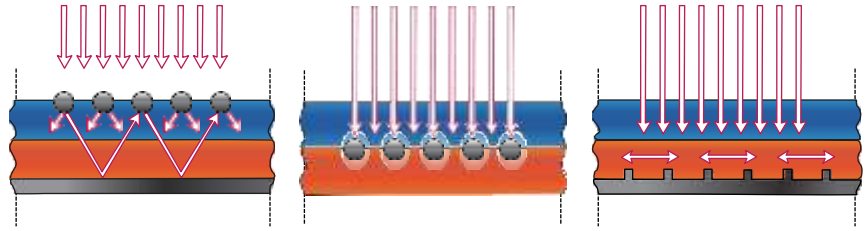

FIGURE 8: Plasmonic light-trapping geometries for thin-film solar cells. (a) Light trapping by scattering from metal nanoparticles at the surface of the solar cell. (b) Light trapping by the excitation of localized surface plasmons in metal nanoparticles embedded in the semiconductor. (c) Light trapping by the excitation of surface plasmon polaritons at the metal/semiconductor interface. Reprinted with permission from [46]. Copyright 2010, Nature Publishing Group.

effectively increasing the optical path length in the cell. In inorganic plasmonic solar cells, the photocurrent enhancement is increased by scattering from metal nanoparticles. Another approach makes use of the near-field enhancement from metal nanoparticles that can be used as subwavelength antennas in which the plasmonic near-field is coupled to the semiconductor, increasing its effective absorption cross-section, as shown in Figure 8(b). In organic plasmonic solar cells, the photocurrent enhancement is increased by near-field enhancement. The direct generation of charge carriers in the semiconductor substrate has also been studied. A corrugated metallic film on the back surface of a thin photovoltaic absorber layer can couple sunlight into surface plasmon polariton (SPP) modes supported at the metal/semiconductor interface as well as guided modes in the semiconductor slab, whereupon the light is converted to photocarriers in the semiconductor as shown in Figure 8(c) [86–88].

Stuart and Hall reported an 18-fold photocurrent enhancement for light-sensitive devices with a 165-nm-thick silicon-on-insulator photodetector at a wavelength of 800 nm by using silver nanoparticles on the surface of the device [89]. The gold nanoparticles used for scattering and absorption of light on highly doped wafer-based solar cells were reported on by Schaadt et al. [90]. Gold nanoparticles on thin-film amorphous silicon solar cells gained an 8% overall increase in conversion efficiency as reported by Derkacs et al. [91]. Silver nanoparticles on 1.25-□m-thick silicon-on-insulator solar cells and planar wafer-based cells obtained 33% and 19% photocurrent increases, respectively, as reported by Pillai et al. [92]. Enhancement in the photocurrent by up to a factor of 2.7 for ITO-copper phthalocyanine-indium structures was reported by Stenzel. Enhancement for silver clusters incorporated in ITO and zinc phthalocyanine solar cells was reported by Westphalen et al. [93]. Enhanced efficiencies for ultrathin film organic solar cells due to 5 nm diameter silver nanoparticles were reported by Rand. An increase in efficiency by a factor of 1.7 for organic bulk heterojunction solar cells was reported by Morfa et al. [94]. Increased photocurrents for CdSe/Si heterostructures [95] and enhanced carrier generation in dye-sensitized solar cells have also been reported [96].

Rho et al. attached TiO_2 nanotube arrays, which were prepared by the electrochemical anodization method, onto a TCO glass to fabricate a transparent photoanode and a front-illuminated DSSC as shown in Figure 9 [47]. With this cell design, the N719 dyes were sensitized more directly by the incident light compared to the conventional back-illuminated DSSCs in which light has to pass through the transparent counter electrode in order to reach the dyes. Ag nanoparticles with diameters smaller than the light wavelength can improve the light absorption dramatically due to the surface plasmon resonance effect. The authors varied the time of exposure to irradiation to examine the Ag nanoparticle deposition kinetics and the existence of the optimal irradiation. The Ag nanoparticles were deposited not only on the outside of the TiO_2 nanotube arrays but also on the inside. The

photovoltaic properties measured for DSSCs without Ag nanoparticles and DSSCs with nanoparticles and varying irradiation times indicated the same tendency. The highest energy conversion efficiency achieved was 6.14%, around 32% improvement of the energy conversion efficiency for DSSCs without Ag nanoparticles, 4.64%. Comparison was also made between front-illuminated and back-illuminated DSSCs. The highest efficiency reported for the back-illuminated DSSCs was 3.077%, which was lower than the front-illuminated DSSCs' highest efficiency. Notably, the effect of incorporating Ag nanoparticles was also lower for back-illuminated DSSCs. The back-illuminated DSSCs showed only a 9.46% increase in

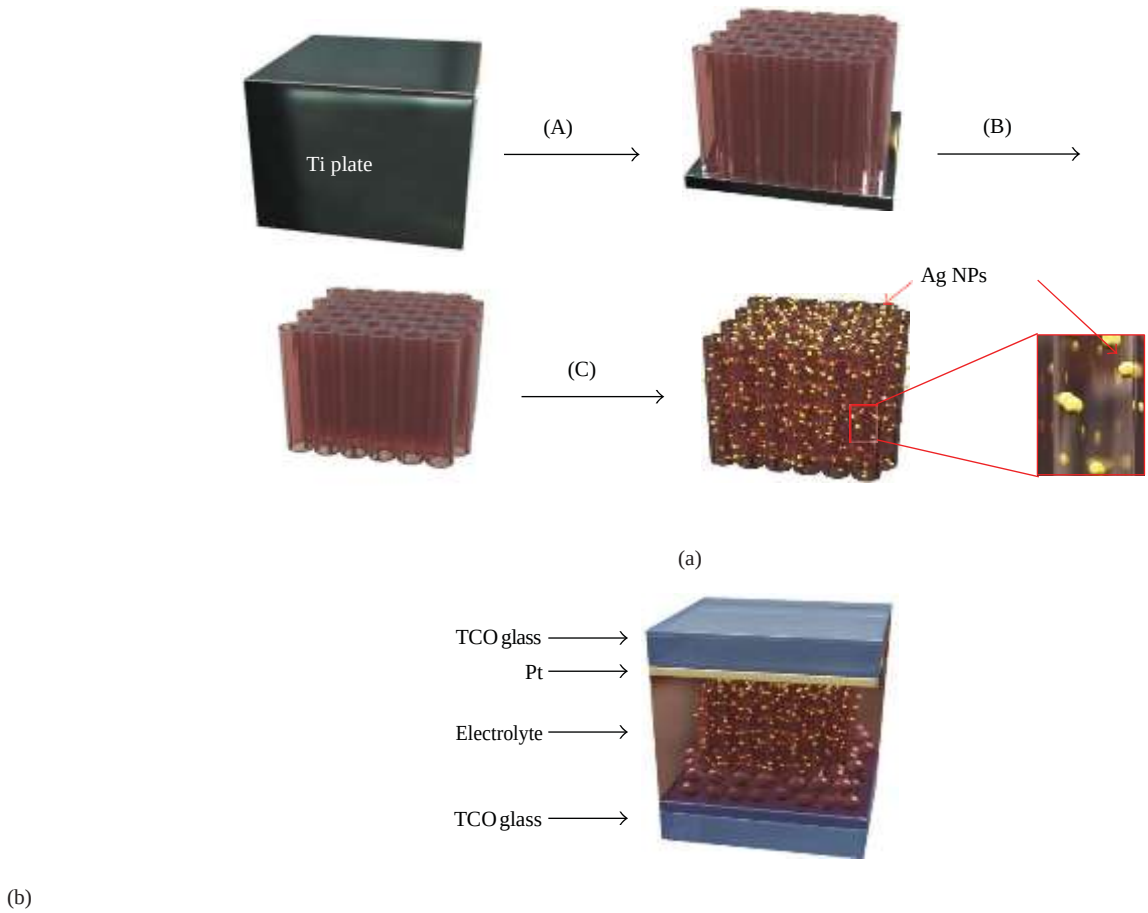

FIGURE 9: (a) Schematic of plasmon DSSC based on method reported by Rho et al. (A) Ti anodization in organic electrolyte, (B) freestanding TiO_2 nanotube arrays, (C) formation of Ag nanoparticles on TiO_2 nanotube arrays by UV irradiation at 254 nm. (b) Schematic of an assembled cell. Reprinted with permission from [47]. Copyright 2014, Elsevier.

the efficiency after the deposition of Ag nanoparticles, which was lower than the 32% increase in the front-illuminated DSSCs. The authors attributed this difference to the reduced intensity of the light passing through the counter electrode and electrolyte layer in the back-illuminated DSSCs, which caused the surface plasmon radiation to occur only at the top part of the TiO_2 nanotube arrays.

(2) $TiCl_4$ with TiO_2 Nanotube Arrays for DSSC Solar Cells. TiO_2 nanoparticles have been deposited to fill the micro-cracks formed in TiO_2 nanotube arrays using an electrophoretic method [97]. By depositing nanoparticles, the conversion efficiency was improved from 4% to 5.2%. Nanoparticles were found in the cracks and on the surface of the nanotubes. The total inner space of the nanotubes might be much larger than the space of the microcracks. However, nanoparticles might not be deposited deep inside the pores. Since TiO_2 nanotube arrays are semiconductors, electrochemical depositions take place at or near the entrances of their pores. There is no driving force to push the deposited nanoparticles into the deep parts of the pores. In vacuum filtering, the solvent provides a driving force, and nanoparticles can be filled throughout the long channels of the TiO_2 nanotube arrays. The TiO_2 nanoparticles that fill the channels of TiO_2 nanotube arrays can make contact with the tubes directly or through other nanoparticles. Since nanotubes are more efficient in electron transfer than are nanoparticles or composites of nanoparticles and nanotubes, electron transfer to the electrode could also be more efficient.

DSSCs based on TiO_2 nanotube arrays filled with TiO_2 nanoparticles have also been fabricated as shown in Figure 10 [48]. The energy conversion efficiency was enhanced by about 21% by filling the channels of the membrane with TiO_2 nanoparticles. By treating with $TiCl_4$ after filling with nanoparticles, the efficiency was enhanced significantly by about 40% due to an increase in the total available surface area for dye adsorption and better electron transfer to the electrode. The method of filling the channels of the TiO_2 membrane with TiO_2 nanoparticles and then treating with $TiCl_4$ was used to improve the energy conversion efficiency of DSSCs based on TiO_2 nanotube arrays.

(3) Additional Layer Technique. Introducing a scattering layer such as TiO_2, ZrO_2, or SiO_2 can increase the total energy conversion efficiency of DSSCs [98]. TiO_2 is a good material to use for a scattering layer due to its chemical stability and

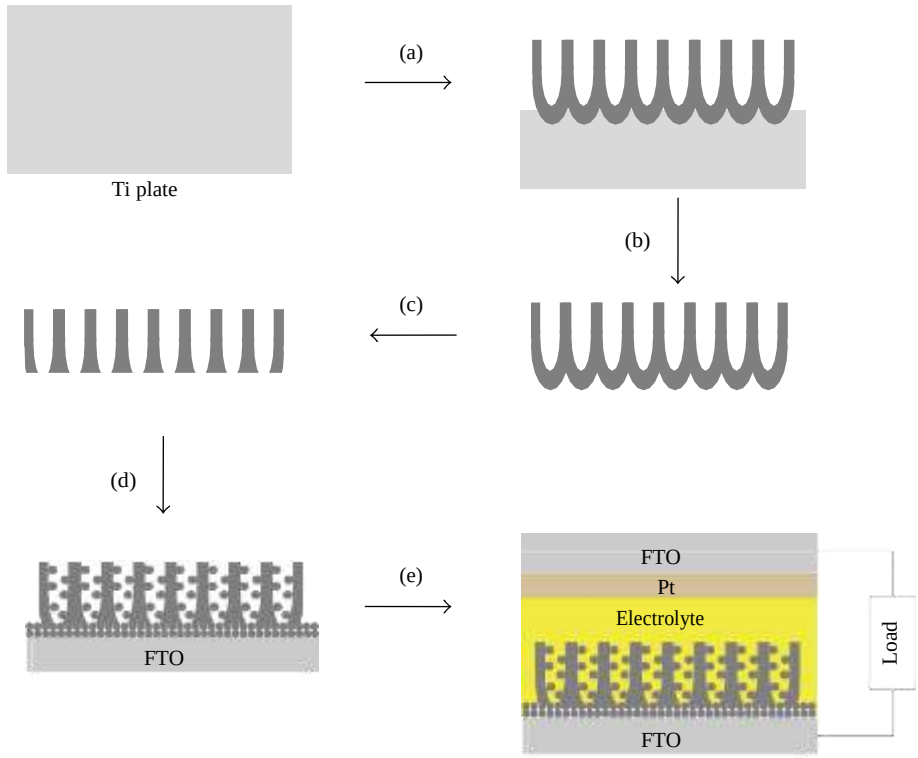

FIGURE 10: Scheme for fabricating a DSSC based on a TiO_2 nanotube membrane filled with TiO_2 nanoparticles: (a) 1st anodization, then annealing, (b) 2nd anodization and detachment of TiO_2 film, (c) ion milling, (d) filling TiO_2 nanoparticles, attaching on fluorine-doped thin oxide (FTO) glass, treating with $TiCl_4$, and then annealing in air, and (e) dye adsorption and fabrication of a DSSC. Reprinted with permission from [48]. Copyright 2011, Elsevier.

dye-adsorption capability; hence, many DSSCs are fabricated using TiO_2 nanoparticle films with a TiO_2 scattering layer on top of the active layer.

Comparison has been made between DSSCs using closed- and open-ended TiO_2 nanotube arrays when a TiO_2 scattering layer is introduced. The energy conversion efficiency was enhanced by 5.15% due to the removal of the barrier layer, which was present in the closed-ended TiO_2 nanotube arrays, causing an improvement in electron transport. By introducing the TiO_2 scattering layer on the open-ended TiO_2 nanotube arrays, the energy conversion efficiency was enhanced by 10.30% due to the improved light harvesting. Additionally, the energy conversion efficiency of the open-ended TiO_2 nanotube arrays treated with $TiCl_4$ was enhanced by 5.51% due to increased dye adsorption. Each component could enhance the DSSC yields.

5. Conclusions and Future Work

In the future, photovoltaic cells will be used in many fields, such as mobile commerce, building integrated photovoltaics (BIPVs), and vehicles. Moreover, photovoltaic cells are essential in the Smart Grid, which is utilized in our daily lives. To apply solar energy in the Smart Grid, photovoltaic cells are required to have transparency, flexibility, light weight, low cost, and high energy conversion efficiency. In terms of low cost and light weight, organics, inorganics, and hybrid materials have brighter prospects than the semiconductors. In hybrid materials, photovoltaic cells have been prepared with the advantages of organics or inorganics selectively. However, it is not easy to increase the energy conversion efficiency. One potential solution is to use 3-dimensional nanostructures, such as nanotubes, nanowires, composite films with metal, or other types of nanostructures. As of today, 0-dimensional nanoparticles in photovoltaic cells still yield the higher energy conversion efficiency by supplying larger surface areas for the sensitizer adsorption. However, the electron transport and flexibility are sufficiently high in 3-dimensional nanostructures. To improve the energy conversion efficiency of 3-dimensional nanostructure based solar cells and take both advantages of 0-dimensional nanoparticles and 3-dimensional nanostructures, the light harvesting ability must be reinforced. One way of achieving the better light harvesting ability is to fill the 0-dimensional nanoparticles in the cavities of 3-dimensional nanostructure, which is another currently active field of study [99].

References

[1] EPA, "Inventory of U.S. greenhouse gas emissions and sinks: 1990–1998," EPA 236-R-00-001, U.S. Environmental Protection Agency, 2000.

[2] *International Engergy Outlook 2013*, U. S. Briefing, 2013.

[3] M. A. Qaeed, K. Ibrahim, K. M. Saron, M. A. Ahmed, and N. K. Allam, "Low-temperature solution-processed flexible solar cells based on (In,Ga)N nanocubes," *ACS Applied Materials & Interfaces*, vol. 6, no. 13, pp. 9925–9931, 2014.

[4] L. Tsakalakos, "Nanostructures for photovoltaics," *Materials Science and Engineering R: Reports*, vol. 62, no. 6, pp. 175–189, 2008.

[5] S. O'Rourke, P. Kim, and H. Polavarapu, *Solar Photovoltaic Industry: Looking through the Storm*, vol. 56, Deutsche Bank, 2009.

[6] T. W. Hamann, R. A. Jensen, A. B. F. Martinson, H. van Ryswyk, and J. T. Hupp, "Advancing beyond current generation dye-sensitized solar cells," *Energy & Environmental Science*, vol. 1, no. 1, pp. 66–78, 2008.

[7] B. O'Regan and M. Grätzel, "A low-cost, high-efficiency solar cell based on dye-sensitized colloidal TiO_2 films," *Nature*, vol. 353, no. 6346, pp. 737–740, 1991.

[8] L. M. Goncalves, V. de Zea Bermudez, H. A. Ribeiro, and A. M. Mendes, "Dye-sensitized solar cells: a safe bet for the future," *Energy & Environmental Science*, vol. 1, no. 6, pp. 655–667, 2008.

[9] M. K. Nazeeruddin, E. Baranoff, and M. Grätzel, "Dye-sensitized solar cells: a brief overview," *Solar Energy*, vol. 85, no. 6, pp. 1172–1178, 2011.

[10] D. Kuang, C. Klein, S. Ito et al., "High-Efficiency and stable mesoscopic dye-sensitized solar cells based on a high molar extinction coefficient ruthenium sensitizer and nonvolatile electrolyte," *Advanced Materials*, vol. 19, no. 8, pp. 1133–1137, 2007.

[11] F. Ribeiro, J. MaçAira, R. Cruz, J. Gabriel, L. Andrade, and A. Mendes, "Laser assisted glass frit sealing of dye-sensitized solar cells," *Solar Energy Materials and Solar Cells*, vol. 96, no. 1, pp. 43–49, 2012.

[12] J. Wu, S. Hao, Z. Lan et al., "An all-solid-state dye-sensitized solar cell-based poly(*N*-alkyl-4-vinyl-pyridine iodide) electrolyte with efficiency of 5.64%," *Journal of the American Chemical Society*, vol. 130, no. 35, pp. 11568–11569, 2008.

[13] W. Wu, J. Li, F. Guo, L. Zhang, Y. Long, and J. Hua, "Photovoltaic performance and long-term stability of quasi-solid-state fluoranthene dyes-sensitized solar cells," *Renewable Energy*, vol. 35, no. 8, pp. 1724–1728, 2010.

[14] J. H. Yum, S. J. Moon, C. S. Karthikeyan et al., "Heteroleptic ruthenium complex containing substituted triphenylamine hole-transport unit as sensitizer for stable dye-sensitized solar cell," *Nano Energy*, vol. 1, no. 1, pp. 6–12, 2012.

[15] T. Kawashima, T. Ezure, K. Okada, H. Matsui, K. Goto, and N. Tanabe, "FTO/ITO double-layered transparent conductive oxide for dye-sensitized solar cells," *Journal of Photochemistry and Photobiology A: Chemistry*, vol. 164, no. 1–3, pp. 199–202, 2004.

[16] J. H. Park, T. W. Lee, and M. G. Kang, "Growth, detachment and transfer of highly-ordered TiO_2 nanotube arrays: use in dye- sensitized solar cells," *Chemical Communications*, no. 25, pp. 2867–2869, 2008.

[17] Q. W. Chen and D. S. Xu, "Large-scale, noncurling, and free- standing crystallized TiO_2 nanotube arrays for dye-sensitized solar cells," *Journal of Physical Chemistry C*, vol. 113, no. 15, pp. 6310–6314, 2009.

[18] C.-J. Lin, W.-Y. Yu, and S.-H. Chien, "Transparent electrodes of ordered opened-end TiO_2-nanotube arrays for highly efficient dye-sensitized solar cells," *Journal of Materials Chemistry*, vol. 20, no. 6, pp. 1073–1077, 2010.

[19] L.-L. Li, Y.-J. Chen, H.-P. Wu, N. S. Wang, and E. W.-G. Diau, "Detachment and transfer of ordered TiO_2 nanotube arrays for front-illuminated dye-sensitized solar cells," *Energy & Environmental Science*, vol. 4, no. 9, pp. 3420–3425, 2011.

[20] R. Buscaino, C. Baiocchi, C. Barolo et al., "A mass spectrometric analysis of sensitizer solution used for dye-sensitized solar cell," *Inorganica Chimica Acta*, vol. 361, no. 3, pp. 798–805, 2008.

[21] M. Grätzel, "Recent advances in sensitized mesoscopic solar cells," *Accounts of Chemical Research*, vol. 42, no. 11, pp. 1788–1798, 2009.

[22] M. K. Nazeeruddin, F. de Angelis, S. Fantacci et al., "Combined experimental and DFT-TDDFT computational study of photoelectrochemical cell ruthenium sensitizers," *Journal of the American Chemical Society*, vol. 127, no. 48, pp. 16835–16847, 2005.

[23] J. Gong, J. Liang, and K. Sumathy, "Review on dye-sensitized solar cells (DSSCs): fundamental concepts and novel materials," *Renewable and Sustainable Energy Reviews*, vol. 16, no. 8, pp. 5848–5860, 2012.

[24] W. Sharmoukh and N. K. Allam, "TiO_2 nanotube-based dye-sensitized solar cell using new photosensitizer with enhanced open-circuit voltage and fill factor," *ACS Applied Materials and Interfaces*, vol. 4, no. 8, pp. 4413–4418, 2012.

[25] D. Kuang, S. Ito, B. Wenger et al., "High molar extinction coefficient heteroleptic ruthenium complexes for thin film dye-sensitized solar cells," *Journal of the American Chemical Society*, vol. 128, no. 12, pp. 4146–4154, 2006.

[26] S. A. Haque, E. Palomares, B. M. Cho et al., "Charge separation versus recombination in dye-sensitized nanocrystalline solar cells: the minimization of kinetic redundancy," *Journal of the American Chemical Society*, vol. 127, no. 10, pp. 3456–3462, 2005.

[27] K. C. D. Robson, B. D. Koivisto, A. Yella et al., "Design and development of functionalized cyclometalated ruthenium chromophores for light-harvesting applications," *Inorganic Chemistry*, vol. 50, no. 12, pp. 5494–5508, 2011.

[28] D. Kuciauskas, J. E. Monat, R. Villahermosa, H. B. Gray, N. S. Lewis, and J. K. McCusker, "Transient absorption spectroscopy of ruthenium and osmium polypyridyl complexes adsorbed onto nanocrystalline TiO_2 photoelectrodes," *Journal of Physical Chemistry B*, vol. 106, no. 36, pp. 9347–9358, 2002.

[29] G. M. Hasselmann and G. J. Meyer, "Sensitization of nanocrystalline TiO_2 by Re(I) polypyridyl compounds," *Zeitschrift für Physikalische Chemie*, vol. 212, part 1, pp. 39–44, 1999.

[30] S. Ferrere, "New photosensitizers based upon [Fe□(L)$_2$ (CN)$_2$] and [Fe□□$_3$L], where L is substituted 2,2-bipyridine," *Inorganica Chimica Acta*, vol. 329, no. 1, pp. 79–92, 2002.

[31] S. Ferrere and B. A. Gregg, "Photosensitization of TiO_2 by [Fe(II)(2,2-bipyridine-4,4-dicarboxylic acid) $_2$(CN)]$_2$; band selective electron injection from ultra-short-lived excited states," *Journal of the American Chemical Society*, vol. 120, no. 4, pp. 843–844, 1998.

[32] S. Ferrere, "New photosensitizers based upon $[Fe(L)_2(CN)_2]$ and $[Fe(L)_3]$ (L = substituted 2,2-bipyridine): yields for the photosensitization of TiO_2 and effects on the band selectivity," *Chemistry of Materials*, vol. 12, no. 4, pp. 1083–1089, 2000.

[33] A. Islam, H. Sugihara, K. Hara et al., "Dye sensitization of nanocrystalline titanium dioxide with square planar platinum(II) diimine dithiolate complexes," *Inorganic Chemistry*, vol. 40, no. 21, pp. 5371–5380, 2001.

[34] E. A. M. Geary, L. J. Yellowlees, L. A. Jack et al., "Synthesis, structure, and properties of [Pt(II)(diimine)(dithiolate)] dyes with 3,3-, 4,4-, and 5,5-disubstituted bipyridyl: applications in dye-sensitized solar cells," *Inorganic Chemistry*, vol. 44, no. 2, pp. 242–250, 2005.

[35] E. A. M. Geary, K. L. McCall, A. Turner et al., "Spectroscopic, electrochemical and computational study of Pt-diimine-dithiolene complexes: rationalising the properties of solar cell dyes," *Dalton Transactions*, no. 28, pp. 3701–3708, 2008.

[36] E. A. M. Geary, N. Hirata, J. Clifford et al., "Synthesis, structure and properties of [Pt(2,2-bipyridyl-5,5-dicarboxylic acid)(3,4-toluenedithiolate)]: tuning molecular properties for application in dye-sensitised solar cells," *Dalton Transactions*, no. 19, pp. 3757–3762, 2003.

[37] S. Sakaki, T. Kuroki, and T. Hamada, "Synthesis of a new copper(I) complex,$[Cu(tmdcbpy)_2]^+$ (tmdcbpy = 4,4,6,6-tetramethyl-2,2-bipyridine-5,5- dicarboxylic acid), and its application to solar cells," *Journal of the Chemical Society, Dalton Transactions*, no. 6, pp. 840–842, 2002.

[38] T. Bessho, E. C. Constable, M. Graetzel et al., "An element of surprise—efficient copper-functionalized dye-sensitized solar cells," *Chemical Communications*, no. 32, pp. 3717–3719, 2008.

[39] M. Alebbi, C. A. Bignozzi, T. A. Heimer, G. M. Hasselmann, and G. J. Meyer, "The limiting role of iodide oxidation in cis-$Os(dcb)_2(CN)_2/TiO_2$ photoelectrochemical cells," *The Journal of Physical Chemistry B*, vol. 102, no. 39, pp. 7577–7581, 1998.

[40] A. Yella, H.-W. Lee, H. N. Tsao et al., "Porphyrin-sensitized solar cells with cobalt (II/III)-based redox electrolyte exceed 12 percent efficiency," *Science*, vol. 334, no. 6056, pp. 629–634, 2011.

[41] M. Zhang, Y. Wang, M. Xu, W. Ma, R. Li, and P. Wang, "Design of high-efficiency organic dyes for titania solar cells based on the chromophoric core of cyclopentadithiophene-benzothiadiazole," *Energy & Environmental Science*, vol. 6, no. 10, pp. 2944–2949, 2013.

[42] S. Qu, W. Wu, J. Hua, C. Kong, Y. Long, and H. Tian, "New diketopyrrolopyrrole (DPP) dyes for efficient dye-sensitized solar cells," *Journal of Physical Chemistry C*, vol. 114, no. 2, pp. 1343–1349, 2010.

[43] S. Minagar, C. C. Berndt, J. Wang, E. Ivanova, and C. Wen, "A review of the application of anodization for the fabrication of nanotubes on metal implant surfaces," *Acta Biomaterialia*, vol. 8, no. 8, pp. 2875–2888, 2012.

[44] G. K. Mor, O. K. Varghese, M. Paulose, K. Shankar, and C. A. Grimes, "A review on highly ordered, vertically oriented TiO_2 nanotube arrays: fabrication, material properties, and solar energy applications," *Solar Energy Materials and Solar Cells*, vol. 90, no. 14, pp. 2011–2075, 2006.

[45] C. Rho, J.-H. Min, and J. S. Suh, "Barrier layer effect on the electron transport of the dye-sensitized solar cells based on TiO_2 nanotube arrays," *Journal of Physical Chemistry C*, vol. 116, no. 12, pp. 7213–7218, 2012.

[46] H. A. Atwater and A. Polman, "Plasmonics for improved photovoltaic devices," *Nature Materials*, vol. 9, no. 3, pp. 205–213, 2010.

[47] W.-Y. Rho, H.-S. Kim, S. H. Lee et al., "Front-illuminated dye-sensitized solar cells with Ag nanoparticle-functionalized freestanding TiO_2 nanotube arrays," *Chemical Physics Letters*, vol. 614, pp. 78–81, 2014.

[48] C. Rho and J. S. Suh, "Filling TiO_2 nanoparticles in the channels of TiO_2 nanotube membranes to enhance the efficiency of dye-sensitized solar cells," *Chemical Physics Letters*, vol. 513, no. 1-3, pp. 108–111, 2011.

[49] M. R. Narayan, "Review: dye sensitized solar cells based on natural photosensitizers," *Renewable and Sustainable Energy Reviews*, vol. 16, no. 1, pp. 208–215, 2012.

[50] R. Nashed, P. Szymanski, M. A. El-Sayed, and N. K. Allam, "Self-Assembled nanostructured photoanodes with staggered bandgap for efficient solar energy conversion," *ACS Nano*, vol. 8, no. 5, pp. 4915–4923, 2014.

[51] J. Z. Ou, R. A. Rani, M.-H. Ham et al., "Elevated temperature anodized Nb_2O_5: a photoanode material with exceptionally large photoconversion efficiencies," *ACS Nano*, vol. 6, no. 5, pp. 4045–4053, 2012.

[52] N.-G. Park, J. van de Lagemaat, and A. J. Frank, "Comparison of dye-sensitized rutile- and anatase-based TiO_2 solar cells," *Journal of Physical Chemistry B*, vol. 104, no. 38, pp. 8989–8994, 2000.

[53] Q. Zhang and G. Cao, "Nanostructured photoelectrodes for dye-sensitized solar cells," *Nano Today*, vol. 6, no. 1, pp. 91–109, 2011.

[54] M. Adachi, Y. Murata, M. Harada, and S. Yoshikawa, "Formation of titania nanotubes with high photo-catalytic activity," *Chemistry Letters*, no. 8, pp. 942–943, 2000.

[55] S.-Z. Chu, S. Inoue, K. Wada, D. Li, H. Haneda, and S. Awatsu, "Highly porous $(TiO_2\text{-}SiO_2\text{-}TeO_2)/Al_2O_3/TiO_2$ composite nanostructures on glass with enhanced photocatalysis fabricated by anodization and sol-gel process," *The Journal of Physical Chemistry B*, vol. 107, no. 27, pp. 6586–6589, 2003.

[56] O. K. Varghese, D. Gong, M. Paulose, K. G. Ong, E. C. Dickey, and C. A. Grimes, "Extreme changes in the electrical resistance of titania nanotubes with hydrogen exposure," *Advanced Materials*, vol. 15, no. 7-8, pp. 624–627, 2003.

[57] G. K. Mor, M. A. Carvalho, O. K. Varghese, M. V. Pishko, and C. A. Grimes, "A room-temperature TiO_2-nanotube hydrogen sensor able to self-clean photoactively from environmental contamination," *Journal of Materials Research*, vol. 19, no. 2, pp. 628–634, 2004.

[58] M. Paulose, O. K. Varghese, G. K. Mor, C. A. Grimes, and K. G. Ong, "Unprecedented ultra-high hydrogen gas sensitivity in undoped titania nanotubes," *Nanotechnology*, vol. 17, no. 2, pp. 398–402, 2006.

[59] O. K. Varghese, G. K. Mor, C. A. Grimes, M. Paulose, and N. Mukherjee, "A titania nanotube-array room-temperature sensor for selective detection of hydrogen at low concentrations," *Journal of Nanoscience and Nanotechnology*, vol. 4, no. 7, pp. 733–737, 2004.

[60] G. K. Mor, K. Shankar, M. Paulose, O. K. Varghese, and C. A. Grimes, "Enhanced photocleavage of water using titania nanotube arrays," *Nano Letters*, vol. 5, no. 1, pp. 191–195, 2005.

[61] G. K. Mor, K. Shankar, O. K. Varghese, and C. A. Grimes, "Photoelectrochemical properties of titania nanotubes," *Journal of Materials Research*, vol. 19, no. 10, pp. 2989–2996, 2004.

[62] O. K. Varghese, M. Paulose, K. Shankar, G. K. Mor, and C. A. Grimes, "Water-photolysis properties of micron-length highly-ordered titania nanotube-arrays," *Journal of Nanoscience and Nanotechnology*, vol. 5, no. 7, pp. 1158–1165, 2005.

[63] S. Uchida, R. Chiba, M. Tomiha, N. Masaki, and M. Shirai, "Application of titania nanotubes to a dye-sensitized solar cell," *Electrochemistry*, vol. 70, no. 6, pp. 418–420, 2002.

[64] M. Adachi, Y. Murata, I. Okada, and S. Yoshikawa, "Formation of titania nanotubes and applications for dye-sensitized solar cells," *Journal of the Electrochemical Society*, vol. 150, no. 8, pp. G488–G493, 2003.

[65] M. Paulose, K. Shankar, O. K. Varghese, G. K. Mor, B. Hardin, and C. A. Grimes, "Backside illuminated dye-sensitized solar cells based on titania nanotube array electrodes (vol 17, pg 1446, 2006)," *Nanotechnology*, vol. 21, no. 38, 2010.

[66] V. Zwilling, M. Aucouturier, and E. Darque-Ceretti, "Anodic oxidation of titanium and TA_6V alloy in chromic media. An electrochemical approach," *Electrochimica Acta*, vol. 45, no. 6, pp. 921–929, 1999.

[67] N. K. Allam, K. Shankar, and C. A. Grimes, "Photoelectrochemical and water photoelectrolysis properties of ordered TiO2 nanotubes fabricated by Ti anodization in fluoride-free HCl electrolytes," *Journal of Materials Chemistry*, vol. 18, no. 20, pp. 2341–2348, 2008.

[68] D. Gong, C. A. Grimes, O. K. Varghese et al., "Titanium oxide nanotube arrays prepared by anodic oxidation," *Journal of Materials Research*, vol. 16, no. 12, pp. 3331–3334, 2001.

[69] G. K. Mor, O. K. Varghese, M. Paulose, and C. A. Grimes, "A self-cleaning, room-temperature titania-nanotube hydrogen gas sensor," *Sensor Letters*, vol. 1, no. 1, pp. 42–46, 2003.

[70] C. Ruan, M. Paulose, O. K. Varghese, and C. A. Grimes, "Enhanced photoelectrochemical-response in highly ordered TiO_2 nanotube-arrays anodized in boric acid containing electrolyte," *Solar Energy Materials & Solar Cells*, vol. 90, no. 9, pp. 1283–1295, 2006.

[71] Q. Y. Cai, M. Paulose, O. K. Varghese, and C. A. Grimes, "The effect of electrolyte composition on the fabrication of self-organized titanium oxide nanotube arrays by anodic oxidation," *Journal of Materials Research*, vol. 20, no. 1, pp. 230–236, 2005.

[72] R. Beranek, H. Hildebrand, and P. Schmuki, "Self-organized porous titanium oxide prepared in H_2SO_4/HF electrolytes," *Electrochemical and Solid-State Letters*, vol. 6, no. 3, pp. B12–B14, 2003.

[73] J. M. MacAk, K. Sirotna, and P. Schmuki, "Self-organized porous titanium oxide prepared in Na_2SO_4/NaF electrolytes," *Electrochimica Acta*, vol. 50, no. 18, pp. 3679–3684, 2005.

[74] M. Paulose, K. Shankar, S. Yoriya et al., "Anodic growth of highly ordered TiO_2 nanotube arrays to 134 □m in length," *Journal of Physical Chemistry B*, vol. 110, no. 33, pp. 16179–16184, 2006.

[75] K. Shankar, G. K. Mor, H. E. Prakasam et al., "Highly-ordered TiO_2 nanotube arrays up to 220 □m in length: use in water photoelectrolysis and dye-sensitized solar cells," *Nanotechnology*, vol. 18, no. 6, Article ID 065707, 2007.

[76] M. Paulose, H. E. Prakasam, O. K. Varghese et al., "TiO_2 nanotube arrays of 1000 □m length by anodization of titanium foil: phenol red diffusion," *Journal of Physical Chemistry C*, vol. 111, no. 41, pp. 14992–14997, 2007.

[77] L. V. Taveira, J. M. Macák, H. Tsuchiya, L. F. P. Dick, and P. Schmuki, "Initiation and growth of self-organized TiO_2 nanotubes anodically formed in $NH_4F/(NH_4)_2SO_4$ electrolytes," *Journal of the Electrochemical Society*, vol. 152, no. 10, pp. B405–B410, 2005.

[78] Z. X. Su and W. Z. Zhou, "Formation mechanism of porous anodic aluminium and titanium oxides," *Advanced Materials*, vol. 20, no. 19, pp. 3663–3667, 2008.

[79] T. P. Hoar and N. F. Mott, "A mechanism for the formation of porous anodic oxide films on aluminium," *Journal of Physics and Chemistry of Solids*, vol. 9, no. 2, pp. 97–99, 1959.

[80] K. R. Hebert, H. Wu, T. Gessmann, and K. Lynn, "Positron annihilation spectroscopy study of interfacial defects formed by dissolution of aluminum in aqueous sodium hydroxide," *Journal of the Electrochemical Society*, vol. 148, no. 2, pp. B92–B100, 2001.

[81] R. Huang, K. R. Hebert, T. Gessmann, and K. G. Lynn, "Effect of impurities on interfacial void formation in aluminum," *Journal of the Electrochemical Society*, vol. 151, no. 4, pp. B227–B232, 2004.

[82] C. Y. Chao, L. F. Lin, and D. D. Macdonald, "A point defect model for anodic passive films. 1. Film growth kinetics," *Journal of the Electrochemical Society*, vol. 128, no. 6, pp. 1187–1194, 1981.

[83] L. F. Lin, C. Y. Chao, and D. D. Macdonald, "A point-defectmodel for anodic passive films .II. Chemical breakdown and pit initiation," *Journal of the Electrochemical Society*, vol. 128, no. 6, pp. 1194–1198, 1981.

[84] J. Meier, S. Dubail, S. Golay et al., "Microcrystalline silicon and the impact on micromorph tandem solar cells," *Solar Energy Materials and Solar Cells*, vol. 74, no. 1-4, pp. 457–467, 2002.

[85] J. Müller, B. Rech, J. Springer, and M. Vanecek, "TCO and light trapping in silicon thin film solar cells," *Solar Energy*, vol. 77, no. 6, pp. 917–930, 2004.

[86] H. A. Atwater and A. Polman, "Plasmonics for improved photovoltaic devices (vol 9, pg 205, 2010)," *Nature Materials*, vol. 9, no. 10, p. 865, 2010.

[87] S. Pillai and M. A. Green, "Plasmonics for photovoltaic applications," *Solar Energy Materials and Solar Cells*, vol. 94, no. 9, pp. 1481–1486, 2010.

[88] K. R. Catchpole and A. Polman, "Plasmonic solar cells," *Optics Express*, vol. 16, no. 26, pp. 21793–21800, 2008.

[89] H. R. Stuart and D. G. Hall, "Island size effects in nanoparticle-enhanced photodetectors," *Applied Physics Letters*, vol. 73, no. 26, pp. 3815–3817, 1998.

[90] D. M. Schaadt, B. Feng, and E. T. Yu, "Enhanced semiconductor optical absorption via surface plasmon excitation in metal nanoparticles," *Applied Physics Letters*, vol. 86, no. 6, Article ID 063106, pp. 1–3, 2005.

[91] D. Derkacs, S. H. Lim, P. Matheu, W. Mar, and E. T. Yu, "Improved performance of amorphous silicon solar cells via scattering from surface plasmon polaritons in nearby metallic nanoparticles," *Applied Physics Letters*, vol. 89, no. 9, Article ID 093103, 2006.

[92] S. Pillai, K. R. Catchpole, T. Trupke, and M. A. Green, "Surface plasmon enhanced silicon solar cells," *Journal of Applied Physics*, vol. 101, no. 9, Article ID 093105, 2007.

[93] M. Westphalen, U. Kreibig, J. Rostalski, H. Lüth, and D. Meissner, "Metal cluster enhanced organic solar cells," *Solar Energy Materials and Solar Cells*, vol. 61, no. 1, pp. 97–105, 2000.

[94] A. J. Morfa, K. L. Rowlen, T. H. Reilly II, M. J. Romero, and J. van de Lagemaat, "Plasmon-enhanced solar energy conversion in organic bulk heterojunction photovoltaics," *Applied Physics Letters*, vol. 92, no. 1, Article ID 013504, 2008.

[95] R. B. Konda, R. Mundle, H. Mustafa et al., "Surface plasmon excitation via Au nanoparticles in n-CdSe/p-Si heterojunction diodes," *Applied Physics Letters*, vol. 91, no. 19, 2007.

[96] C. Hägglund, M. Zäch, and B. Kasemo, "Enhanced charge carrier generation in dye sensitized solar cells by nanoparticle plasmons," *Applied Physics Letters*, vol. 92, no. 1, Article ID 013113, 2008.

[97] K. Shin, Y. Jim, G. Y. Han, and J. H. Park, "Effect of incorporation of TiO_2 nanoparticles into oriented TiO_2 nanotube based dye-sensitized solar cells," *Journal of Nanoscience and Nanotechnology*, vol. 9, no. 12, pp. 7436–7439, 2009.

[98] . Hore, C. Vetter, R. Kern, H. Smit, and A. Hinsch, "Influence of scattering layers on efficiency of dye-sensitized solar cells," *Solar Energy Materials and Solar Cells*, vol. 90, no. 9, pp. 1176–1188, 2006.

[99] J. Maçaira, L. Andrade, and A. Mendes, "Review on nanostructured photoelectrodes for next generation dye-sensitized solar cells," *Renewable and Sustainable Energy Reviews*, vol. 27, pp. 334–349, 2013.